Mesoscale structure of diffusion-limited aggregates of colloidal rods and disks

Jacob R. Rothenbuhler,[a] Jung-Ren Huang,[b] Brian A. DiDonna,[b] Alex J. Levine[c] and Thomas G. Mason*[d]

Received 18th May 2009, Accepted 20th July 2009
First published as an Advance Article on the web 13th August 2009
DOI: 10.1039/b909740f

We explore the dependence of the non-universal mesoscale structure of diffusion-limited aggregates upon the shape of their constituent particles. Using random-walker simulations that model anisotropic diffusion in a viscous fluid, we study diffusion-limited aggregation (DLA) of right-circular cylinders having a wide range of length-to-diameter aspect ratios. This single-parameter family of particle shapes allows us to determine the role of particle *quasi-dimensionality* on the structure of DLA clusters that are composed of effectively one-dimensional thin rods and two-dimensional thin plates. We compare these clusters to those formed by traditional DLA of compact objects by studying the local nature of the interparticle contacts (end–end, end–body, or body–body), the distribution of the number of interparticle contacts, and the wavevector-dependent structure factor $S(q)$ of the resulting clusters. We find that clusters of rods are less dense than those of disks or compact objects of equal volume, yet the long length-scale structure of the DLA clusters conforms to the expected DLA scaling relations. However, the local structure at the particle scale, including the nearest-neighbor distribution functions and dominant collision types, depend strongly on the particle's quasi-dimensionality. We explain the non-universal local structure by introducing the concept of a diffusing particle's 'touch space', which incorporates both the particle's geometry and its anisotropic diffusion.

1 Introduction

It is well-known that strong interparticle attractions can destabilize colloidal dispersions, thereby causing particle aggregation. If interparticle attractions are much stronger than thermal energy and act only at short range, when diffusing particles collide, the *nonequilibrium* multiparticle structures formed at vanishingly low particle densities are diffusion-limited aggregates.[1,2] Due to the strength of the interparticle bonding, the average internal structure of these aggregates reflects the diffusive dynamics of individual particles, which randomly approach the growing cluster and then bond irreversibly upon first contacting it. While these conditions might appear to be difficult to find in nature, such nonequilibrium growth processes driven by diffusive transport actually abound, and the resulting aggregates are ubiquitous. DLA can be seen in dispersions of soot,[3] the flocculation of organic and mineral deposits in the sea,[4] and even in condensation kinetics of the early solar nebula.[5]

Large DLA clusters containing many spherical particles are visually striking, tenuous networks of bonded particles. The cluster-scale properties of these structures are, in fact, universal and have been extensively studied since their initial classification and characterization.[1,2] Examples of universality in DLA structures include their self-affinity[6,7] and their mass-scaling relationship; the total mass of particles contained within a DLA cluster scales as a power law of distance from its center with a universal power law exponent, or *fractal dimension*, of $d_f \approx 2.4$ to 2.5. DLA differs from another well-known process known as diffusion-limited cluster aggregation (DLCA), in which growing clusters are allowed to diffuse and collide, yielding a smaller effective fractal dimension.

Classic studies of DLA have analyzed spherical particles that diffuse isotropically in space until they collide with the growing cluster; they then stick at contact to form shear-rigid bonds. Some variations of this basic growth mechanism have been explored. Allowing lubricated slip at interparticle contacts alters the local nearest-neighbor distributions; such *slippery* diffusion-limited aggregates are effectively composed of compact corrugated clusters, but retain the same fractal dimension when examined at the cluster scale.[8,9] This change in local structure has been observed in neutron scattering from aggregates of spherical nanoemulsion droplets.[9,10] Anisotropic stickiness of spheres can also influence DLA structures[11–13] leading to locally more linear structures than those found using the regular DLA model. When combined with symmetry-breaking orientational biasing of the random-walkers, anisotropic stickiness can lead to the formation of long needle-like aggregates with a long-scale-length universal mass-scaling exponent of 2/3, instead of the usual result.[14]

In this study, we explore how the local connectivity and mesoscale structure of DLA clusters depends on the shape or *quasi-dimensionality* (*qD*) of the constituent particles. Quasi-dimensionality of an anisotropic object is defined to be the dimensionality of the subspace spanning the directions in which the object's linear extent is significantly larger than its shortest spanning length. Thus, long thin rods are quasi-one-dimensional and plates are quasi-two-dimensional. For nearly isotropic objects having no such large separation of length scales, there is

[a]*Department of Physics & Astronomy, University of California, Los Angeles, CA 90095, USA*
[b]*Department of Chemistry & Biochemistry, University of California, Los Angeles, CA 90095, USA*
[c]*Department of Chemistry & Biochemistry, California NanoSystems Institute, University of California, Los Angeles, CA 90095, USA*
[d]*Department of Physics & Astronomy, Department of Chemistry & Biochemistry, California NanoSystems Institute, University of California, Los Angeles, CA 90095, USA. E-mail: mason@physics.ucla.edu*

a remaining ambiguity: they can be equally well considered to be quasi-zero-dimensional or quasi-three-dimensional. We choose the latter description. Recent advances in synthetic chemistry and the ability to isolate nanoscale biological structures have opened up the possibility of exploring the formation of DLA clusters of plates (2D structures) and long rods (1D structures), in addition to the well-studied spheres (compact 3D structures). Examples of such rod-like colloidal particles include nanowires,[15] nanorods,[16,17] and microtubules[18] as well as monodisperse viruses.[19] Similarly, nanodisks[20] and microdisks[21] have been created.

It might be anticipated that clusters composed of particles having varying quasi-dimensionality would obey the universal scaling characteristics of DLA at the cluster scale. However, at mesoscopic length scales larger than the typical particle size, yet smaller than where these universal asymptotics applies, one expects to observe the effect of particle shape on the local connectivity of the particles and on the local structure of the aggregates, due to both the locally anisotropic diffusion of the motile particle and the varying size of the phase space for interparticle collision as a function of relative orientation. Through simulations, we examine the complex mesoscale structure created by DLA of highly anisotropic particles, and we understand the resulting non-universal mesoscale structure of the clusters by introducing the *touch space* of a particle. The touch space of a diffusing particle is defined as the volume of space swept out around the particle with probability greater than e^{-1} in a time sufficient for the diffusion of the center of mass of the particle by its shortest spanning length. This touch space is a measure of how effectively the particle diffusively searches its local environment for potential interparticle contacts before translating significantly. An example of the touch space of a long, thin rod is shown in Fig. 1, where we see that the ends of the rod explore a proportionately larger volume of space than its cylindrical body.

In order to explore the role of particle quasi-dimensionality in DLA, we use numerical simulations of monodisperse rigid right-circular cylinders having flat and solid end-caps in the limit of extremely low particle density. Upon contact with the cluster, they instantaneously form shear-rigid bonds. Such nonequilibrium aggregates of strongly attractive rods have already been examined in the high particle density limit[22] where cluster–cluster interactions form a gel (*i.e.* a system-spanning network) through diffusion-limited cluster aggregation (DLCA), which was earlier identified for spheres.[23–25] By varying the aspect ratio of the cylinders, *i.e.* their length-to-diameter ratio, α, over a few orders of magnitude we explore particle quasi-dimensionalities from long rods ($\alpha \gg 1$, $qD = 1$) to nearly isotropic, short cylinders ($\alpha \simeq 1$, $qD = 3$) to thin disks ($\alpha \ll 1$, $qD = 2$). Although anisotropic rotational and translational diffusion coefficients are not known exactly as a function of α, we estimate these from Stokes drag calculations based on limiting cases.

We show that given equal particle volume, aggregates composed of ($qD = 1$) long rods are quite tenuous, aggregates of stubby cylinders ($qD = 3$) resemble classic DLA, and aggregates of quasi-two-dimensional thin disks ($qD = 2$) are intermediate in average density. Independent of aspect ratio or qD, all DLA clusters of cylinders have $d_f = 2.4 \pm 0.1$ for length scales much larger than the maximum dimension of the cylinder, consistent with DLA of spheres. However, the nearest-neighbor distributions of clusters made from rod-like constituents can differ significantly from classic DLA. Moreover, the statistics of collision types reflect a predominance of collisions involving at least one end of a cylinder. To provide a connection to scattering experiments, we calculate the wavenumber-dependent average scattering intensity $I(q)$ and structure factor $S(q)$ resulting from coherent scattering by finite-size fractal aggregates of cylinders. Moreover, we identify hallmark features in the scattering functions that can be used to distinguish fractal clusters made of rod-like, compact, and plate-like constituent particles.

The remainder of the paper is organized as follows. In section 2 we discuss our numerical growth model for highly anisotropic particles. In section 3 we analyze the statistical properties of the structure of the resulting aggregates as a function of length scale, before concluding in section 4.

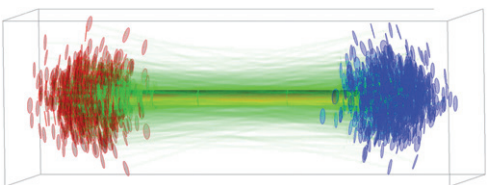

Fig. 1 Touch space rendering of a rod-like cylinder having length-to-diameter aspect ratio $\alpha = 20$. The horizontal rod (yellow) is the starting cylinder position. After the rod diffuses over a short time period, we record the end cap locations (blue and red disks) and a semi-transparent green line that connects the centers of end-caps By superimposing the results of 1000 trials, the green region and the scattered pockets of blue and red qualitatively depict the probabilistic collisional space explored by the cylinder body and end-caps, respectively.

2 Model

We have performed off-lattice, three-dimensional, random-walker simulations to grow DLA clusters composed of uniform right circular cylinders of length L and radius a, having a fixed aspect ratio $\alpha = L/(2a)$ and a volume $V = \pi a^2 L$. To generate DLA clusters, we set R_{max} to be the maximum of the distances from the center of mass of the growing cluster to the center of each particle. Initially, this distance is zero when a single immobile cylinder is placed at the origin to start the growth process. Subsequently, a single mobile cylinder is released away from the growing cluster at a randomly chosen point on the surface of a sphere of radius $R_{release} = R_{max} + \ell$, where ℓ is longest linear dimension of a single particle. Once released, this particle diffuses anisotropically through a viscous fluid until it either collides with the growing cluster and rigidly sticks, or it diffuses away from the cluster to the elimination distance, $R_{elim} \approx 4R_{max}$ and is abandoned. If a collision is detected, the diffusing cylinder's position and orientation at contact are recorded. We choose the time step δt of the Brownian dynamics of the single motile cylinder to be small enough to prevent it from making multiple collisions with the growing cluster. For each collision detected, we eliminate partial–particle overlaps by backing up the motile particle until the only the two cylinders barely touch. We repeat this process of releasing and tracking

single diffusing cylinders until the cluster contains the desired number N of cylinders.

The simulated random walk of the motile cylinder must take into account the anisotropic mobility of the object. For each δt, we update the center-of-mass position of the cylinder by $\delta\mathbf{x} = \delta x_{\|}\hat{n} + \delta x_{\perp}\hat{x}_{\perp}$, where $\delta x_{\|,\perp}$ represents respectively the displacements along the cylinder's axis $\hat{n}$ and perpendicular to it, $\hat{n}\cdot\hat{x}_{\perp} = 0$. These stochastic variables are chosen from Gaussian distributions both having zero mean and whose second moments are given by $\langle \delta x_{\|}^2 \rangle = 2D_{\|}\delta t$ and $\langle \delta x_{\perp}^2 \rangle = 4D_{\perp}\delta t$, where $D_{\|}$ and $D_{\perp}$ are the translational diffusion coefficients along the cylinder's axis and perpendicular to it, respectively[26] [eqns (1), (3), and (4)]. To account for the rotational diffusion of the rod, we alternate making translational steps with rotational steps. Each rotational step is determined by: $\delta\hat{n} = \delta\psi\hat{\omega} \times \hat{n}$, where unit vector $\hat{\omega}$, the axis of rotation, is chosen randomly in the plane orthogonal to $\hat{n}$ and the rotation angle is another stochastic variable selected from a Gaussian distribution having zero mean and a second moment given by $\langle \delta\psi^2 \rangle = 4D_{\mathrm{R}}\delta t$, where D_{R} defines the rotational diffusion constant[26] [eqns (2) and (5)].

Although anisotropic diffusion coefficients for cylinders in certain limiting cases are known, and a related theory for ellipsoids exists,[26] the general formulae as a function of α are not known precisely. For a given α, we estimate the anisotropic diffusion coefficients as follows. For rods having $\alpha > 1$, we adopt the hydrodynamic friction coefficients $\zeta_{\|}$, $\zeta_{\perp}$, and ζ_{R} in Kirkwood's theory for $\alpha \gg 1$.[26,27] Stokes–Einstein relation ($D = k_{\mathrm{B}}T/\zeta$) then leads to

$$D_{\|} = 2D_{\perp} = \frac{k_{\mathrm{B}}T}{2\pi\eta L}\log(\alpha) \tag{1}$$

$$D_{\mathrm{R}} = \frac{3k_{\mathrm{B}}T}{\pi\eta L^3}\log(\alpha/2) \tag{2}$$

where η is the viscosity of the solvent, k_{B} is Boltzmann's constant, and T is the temperature. Diffusion along a long rod's axis is twice as fast as perpendicular to it. By the same token, for disks having $\alpha < 1$, we take $\zeta_{\|}$, $\zeta_{\perp}$, and ζ_{R} from the low-frequency Stokes flow result of Zhang and Stone for $\alpha \ll 1$.[28] The diffusion coefficients, therefore, are given by

$$D_{\|} = \frac{k_{\mathrm{B}}T}{8\eta V^{1/3}}(\pi\alpha/4)^{1/3} \tag{3}$$

$$D_{\perp} = \frac{3k_{\mathrm{B}}T}{16\eta V^{1/3}}(\pi\alpha/4)^{1/3} \tag{4}$$

$$D_{\mathrm{R}} = \frac{3k_{\mathrm{B}}T}{4\eta V}(\pi\alpha/4) \tag{5}$$

Diffusion along a thin disk's axis is about one and a half times slower than edge-wide diffusion. For stubby cylinders having $\alpha = 1$, we model the translational diffusion as effectively being isotropic: $D_{\|} = D_{\perp}$. To speed up the diffusion routine, when the cylinder is more than three times its maximum dimension away from the nearest particle in the cluster, the cylinder diffuses isotropically; parallel and perpendicular particle mobilities are set equal, and we do not introduce or track rotational diffusion. Once the particle approaches the cluster, we randomize its orientation and return to the full simulation of its anisotropic diffusive dynamics. We have verified that this simplification does not affect the resulting aggregate structures, as compared to the rigorous application of the diffusive dynamics over all time steps.

By generating sets of clusters having up to $N = 50\,000$ particles over $10^{-2} \leq \alpha \leq 10^{2}$, we explore how the quasi-dimensionality of a uniform building block can influence DLA structures. In Fig. 2 we show representative DLA clusters of cylinders: (a) long rods having $\alpha = 20$, (b) stubby cylinders having $\alpha = 1$, and (c) thin disks having $\alpha = 0.05$. Clusters composed of long rods are significantly more tenuous than those composed of either thin disks or stubby cylinders, which form the most compact structures. The clusters are color-coded based on the order of release of the cylinders. Cylinders released at a later time adhere to the extremities of the cluster preferentially rather than penetrate deep within it. Thus, the screening of the interior of the cluster by growing arms in classic DLA is seen for cylinders, too. The insets of Fig. 2 show detailed close-up views of local cylinder configurations that are typical at the outer arms of the aggregates. Body–body collisions are preferred for very long rods, whereas end–end collisions are dominant for thin disks. Comparing the local structures at the extremities, it appears that long rods are attached to DLA clusters more frequently by a single bond than lower-aspect-ratio particles.

3 Results

To determine the fractal dimensions of the clusters, we calculate the number of cylinders (*i.e.* their total volume V_{T} which is proportional to their total mass) within an imaginary test sphere having radius r centered at the center-of-mass of the cluster. We expect to find a power-law dependence $V_{\mathrm{T}} \sim r^{d_{\mathrm{f}}}$ allowing us to extract the so-called mass-scaling dimension.[1] We scale distances by $V^{1/3}$, a characteristic linear dimension related to the cylinder volume, to provide a common basis for comparing cluster sizes having different α. This choice allows us to vary α at fixed particle volume. Clearly a uniform change of scale of the particles makes a trivial rescaling of characteristic lengths of their aggregates. Furthermore, in the case of long rods, we decompose the mass of each rod into a set of smaller stubby cylinders and count the number of these smaller cylinders to provide a more accurate measure of the mass distribution at short distances, $r < L$. Independent of α, for larger $r/V^{1/3} > 10$, the mass-scaling exponent is found to be $d_{\mathrm{f}} = 2.4 \pm 0.1$, similar to classic DLA of spheres [Fig. 3(a)].[29] For long rods, there is a crossover to a well-defined scaling regime having $d_{\mathrm{f}} = 1$ at small r, reflecting the essentially one-dimensional mass distribution of the rods at short distances. By the same reasoning, we expect clusters of disks to show a cross-over from the fractal dimension scaling $d_{\mathrm{f}} = 2.4$ to $d_{\mathrm{f}} = 2$ reflecting their two-dimensional nature at small r. For all α, the fractal mass-scaling regime ends at length scales comparable to the radius of gyration of the clusters, R_{g} (Fig. 3(a) inset). Examining the ratio of $R_{\mathrm{g}}/V^{1/3}$, we find that the clusters are most compact for $\alpha = 1$, corresponding to stubby 3D cylinders. This curve is not symmetric about $\alpha = 1$ on the log scale: clusters made up of quasi-1D long rods are more tenuous and extended than clusters of quasi-2D thin disks. When r is scaled by R_{g}, the mass-scaling curves for all cylinders collapse into a single master curve

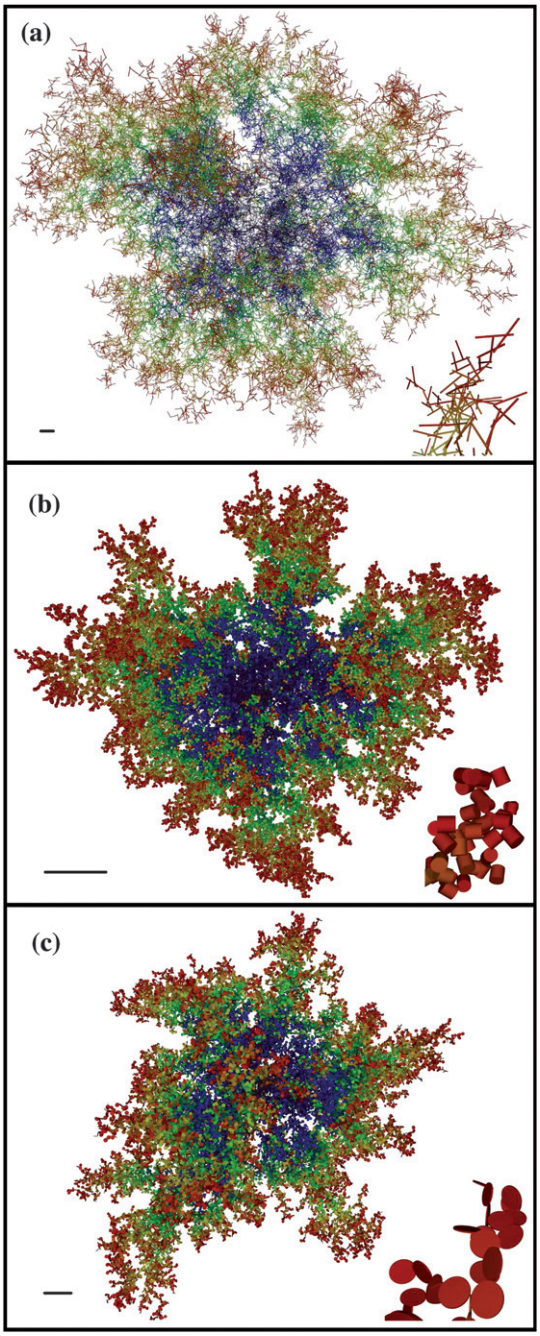

Fig. 2 Diffusion-limited aggregates containing $N = 50\,000$ right-circular cylinders having length-to-diameter aspect ratios $\alpha = L/(2a)$: (a) 20 (quasi-1D or rod-like), (b) 1.0 (compact-3D or isotropic), and (c) 0.05 (quasi-2D or disk-like). Colors of particles indicate the order of aggregation from first to last (blue–green–yellow–orange–red). Scale bars (lower left) indicate approximate relative sizes of clusters for cylinders having the same volume. Insets (lower right): detailed particle-scale structures of terminal arms of the aggregates.

for lengths in the fractal scaling regime between $V^{1/3}$ and R_g [Fig. 3(b)].

Particle-scale structures within the aggregate of cylinders also depend on α. To study those structures, we separate each inter-particle contact into one of three groups, depending upon the type of collision. Body–body (BB) contacts occur when the

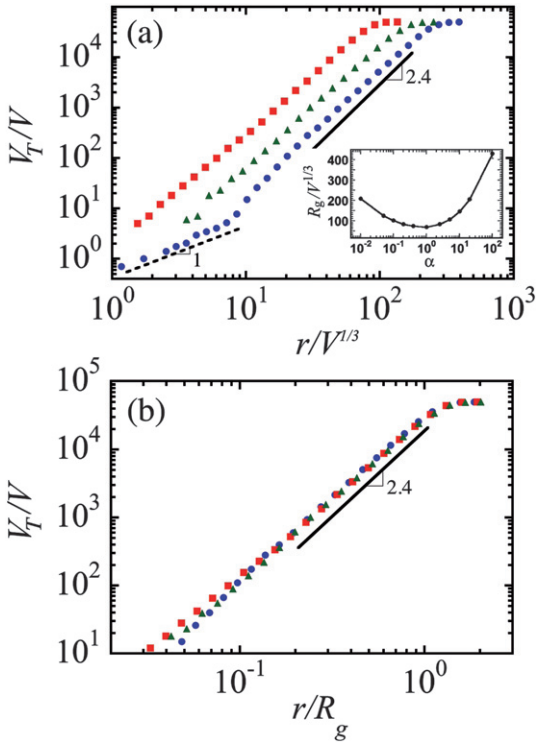

Fig. 3 Nondimensionalized volume V_T/V, of right-circular cylinders in diffusion-limited aggregates enclosed within a sphere having radius: (a) $r/V^{1/3}$ for cylinders having volume V and aspect ratios $\alpha = 0.05$ (triangles), 1 (squares), and 20 (circles). The solid line indicates a log slope of 2.4, and the dashed line at smaller $r/V^{1/3}$ indicates a linear scaling due to the rod-like cylinders. (b) r/R_g where R_g is the radius of gyration of the cluster. The inset in (a) shows $R_g/V^{1/3}$ as a function of α.

cylindrical surface of one particle touches the cylindrical surface of another. End–body (EB) contacts occur when one of the flat circular end-caps of a particle touches the cylindrical surface of another. Finally, end–end (EE) contacts occur when the flat end-caps of two particles touch. To resolve any ambiguity in assigning the contact type, both circular edges (*i.e.* rims) of any cylindrical particle are assigned to its ends. Thus, if a circular edge contacts any part of the end-cap of another cylinder, this contact is considered to be of the end–end variety. We plot the probability distributions of these collision types, $p_{EE}(\alpha)$, $p_{EB}(\alpha)$, and $p_{BB}(\alpha)$, in Fig. 4. End–end collisions dominate for thin disks, but such collisions become rare for aggregates of long thin rods. Thus, p_{EE} monotonically decreases from one to zero as α increases. Likewise, p_{BB} increases from nearly zero for thin disks and approaches unity for rods ($\alpha \gg 1$). Consequently, conservation of probability, $p_{EE} + p_{EB} + p_{BB} = 1$, requires that p_{EB} vanishes in the limits of $\alpha \to 0, \infty$. Indeed, we find that p_{EB} starts near zero for thin disks, goes through a maximum at $\alpha \simeq 6$, and decreases again towards zero for long rods.

Assuming that the contact probability over the surface of the motile particle is independent of position on it, one might naively expect that the relative frequencies of collision types should occur in proportion to the area fraction of the particles' ends or bodies. We refer to this as the *uniform probability assumption* (UPA). A calculation based on the simple UPA, however, strongly overestimates the frequency of body–body collisions,

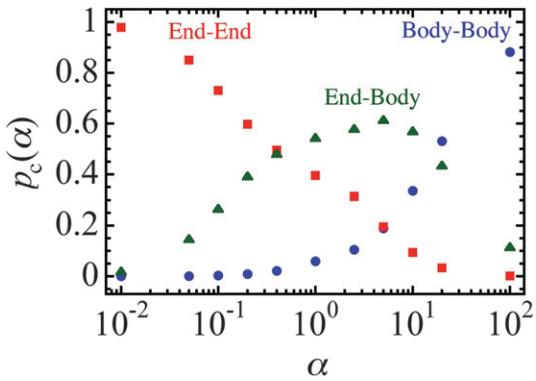

Fig. 4 Relative collision probabilities p_c of the following collision types for 50 000 particle aggregates as a function of cylinder aspect ratio α: end–end p_{EE} (red squares), end–body p_{EB} (green triangles), and body–body p_{BB} (blue circles).

and the α-dependence of the body–body collision frequency predicted by this calculation disagrees with the numerical data. For small α, the probability of body–body collisions grows more slowly than the UPA model predicts. Simulation data shows that $p_{BB} \simeq 0.1\alpha^{3/2}$, whereas the simple UPA leads to an α^2 growth for this quantity. However, for long rods, the simple UPA predicts that $p_{BB} \sim 1 - 1/\alpha$; this appears to be supported by the numerical data. The model based on UPA also incorrectly predicts p_{EE}. To summarize, the UPA model overestimates the frequency of body–body collisions and underestimates the frequency of end-type collisions.

We hypothesize that the particles' anisotropic diffusion is the primary source of the failure of the UPA model. In particular, the ends of long rods explore a much greater volume of space than their bodies. Due to both enhanced longitudinal translational diffusion and rotational fluctuations about the cylinders' center of mass, the cylinders' ends explore a touch space in search of collisions of a significantly larger volume than the UPA model predicts. For long rods, this touch space is shaped like a dumbbell (Fig. 1), whereas for thin disks, the touch space is shaped in a form resembling an oblate lozenge. We speculate that this dynamic touch-space enhancement is the source of the pronounced shift towards end-type collisions that causes the maximum of p_{EB} to occur at $\alpha \approx 6$, rather than $\alpha \approx 1$.

We also calculate the nearest-neighbor distribution $p_z(z)$ of the number of contacts z that a particle makes with other particles. In Fig. 5(a), as the aspect ratio changes from the limit of a stubby cylinder to a long rod, $p_z(z)$ changes from the classic DLA result with a peak at $z = 2$ to a strikingly different curve. As $\alpha \gg 1$, the maximum occurs at $z = 1$ and decreases monotonically towards higher z. The maximum at $z = 1$ indicates that most of the particles in the cluster have only one bond with a neighboring particle. This represents a predominance of one-dimensional hair towards the extremities of the cluster. Furthermore, as α becomes very large, there is a systematic rise in the number of rods that have high branching numbers $z > 3$ (Fig. 5(a) inset). Non-zero probabilities at such high branching numbers have never been found for compact objects such as stubby cylinders or spheres. As α decreases from unity towards the limit of thin disks [Fig. 5(b)], $p_z(z)$ changes very little, so aggregates resulting from

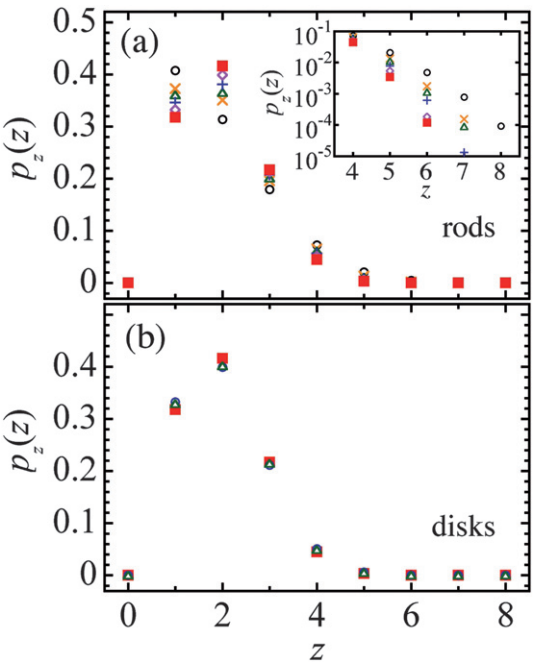

Fig. 5 Probability distributions $p_z(z)$ of the number of nearest neighbors z in an aggregate of 50 000 particles for a series of aspect ratios: (a) rod-like cylinders: α = 100 (○), 20 (×), 10 (△), 5 (+), 1 (■); (b) disk-like cylinders: α = 1 (■), 0.1 (△), 0.01 (○).

quasi-2D platelets have very similar nearest-neighbor distributions to classic diffusion-limited aggregates of 3D objects.

The structure factor[30] of DLA clusters composed of isotropic (point-like) particles has been computed in detail previously[31] and the subject of much experimental investigation using X-ray, neutron[32] and light scattering.[33] In order to relate our real-space results of cylinder DLA to such experiments, we calculate the intensity I and the structure factor S as a function of scattering wavevector $\mathbf{q}$, assuming monochromatic plane wave illumination and a wavelength that is much smaller than any length scale associated with the cylinders or cluster.[30] Experimentally, when scattering from a dilute solution of such clusters, one obtains the incoherent sum of scattering from clusters of many different sizes, orientations, or numbers of particles. The un-normalized scattering intensity $I(q)$ and the structure factor $S(q)$ are therefore given by

$$I(q) = \left\langle \left| \sum_{j=1}^{N} f_j(\mathbf{q}) \exp[i\,\mathbf{q}\cdot\mathbf{r}_j] \right|^2 \right\rangle$$

$$S(q) = \left\langle \left| \sum_{j=1}^{N} \exp[i\,\mathbf{q}\cdot\mathbf{r}_j] \right|^2 \right\rangle$$

where $q = |\mathbf{q}|$, N is the number of particles in a single cluster, and $\mathbf{r}_j$ is the center-of-mass position of the j-th particle. The particle's form factor amplitude $f_j(\mathbf{q}) = \int_{\mathbf{r}\in V(j)} d^3\mathbf{r} \exp[i\,\mathbf{q}\cdot\mathbf{r}]$, where the integration is performed over its volume $V(j)$. The form factor $|f_j(\mathbf{q})|^2$ varies with the orientation of the particle.[34] The angled brackets $\langle\cdot\rangle$ represent both ensemble and orientation averages. Due to the computational effort required to create new clusters, for a given α, we calculate $I(q)$ and $S(q)$ by averaging over at least

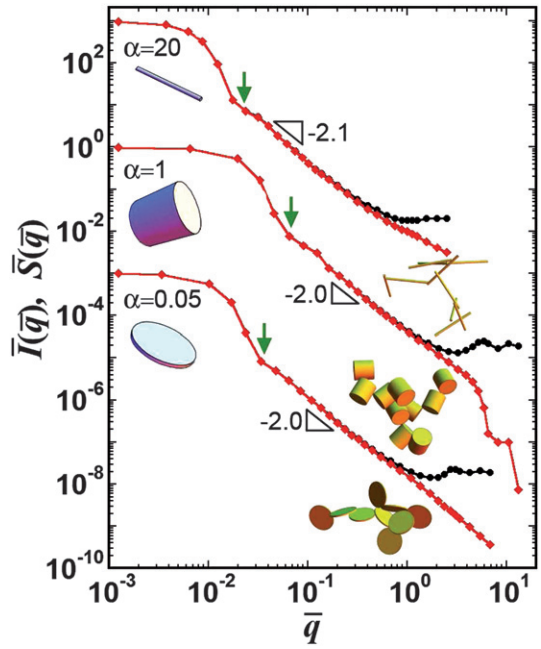

Fig. 6 Normalized scattering intensities $\bar{I}(\bar{q}) = I(q)/(N^2V^2)$ (red diamonds) and structure factors $\bar{S}(\bar{q}) = S(q)/N^2$ (black dots) of the aggregates composed of $N = 50\,000$ particles having aspect ratios $\alpha = L/(2a) = 0.05$, 1, and 20 (bottom to top) for fixed cylinder volume V, where $\bar{q} = qV^{1/3}$. Results for $\alpha = 0.05$ and 20 are multiplied by 10^{-3} and 10^3, respectively. Arrows mark the locations of $\bar{q} = \bar{q}_{gf} = 3\pi V^{1/3}/(2R_g)$, where R_g denotes the aggregate's average radius of gyration. For $\bar{q}_{gf} = q_{gf}V^{1/3} < \bar{q} < 1$, both $I(\bar{q})$ and $S(\bar{q}) \sim \bar{q} - 2$. Images show the particle geometry (left) and an example of the first 10 aggregated particles in a cluster (right).

four independently-generated monodisperse clusters, and use 350 orientations of each cluster. We find that a rotationally averaged cylinder form factor $\langle|f_j(\mathbf{q})|^2\rangle$ appropriately describes cylinder-scale scattering, suggesting that there are no correlations between the orientation of a cylinder and its center-of-mass position with respect to the center of the cluster.

Fig. 6 shows the normalized scattering intensity $\bar{I}(\bar{q})$ and structure factor $\bar{S}(\bar{q})$, where $\bar{q} = qV^{1/3}$ is the dimensionless wavenumber, for clusters composed of thin disks, stubby cylinders, and long rods. At the lowest $\bar{q}$, $\bar{I}(\bar{q})$ and $\bar{S}(\bar{q})$ are almost indistinguishable. When $\bar{q} \leq 1$, the form factor amplitude is about equal to the cylinder volume V and, therefore, $\bar{I}(\bar{q}) \simeq \bar{S}(\bar{q})$. The pronounced knee (see green arrows) for $\bar{q}$ near $\bar{q}_{gf} = 3\pi V^{1/3}/(2R_g)$ distinguishes the lower-$\bar{q}$ Guinier regime[35] from the apparent fractal regime at higher $\bar{q}$ ($\bar{q}_{gf} < \bar{q} < 1$). This knee indicates the finite extent of the cluster in reciprocal space. Consequently, $\bar{I}$ for a large cluster composed of rods having $\alpha \gg 1$ exhibits a knee at lower $\bar{q}$.

At intermediate $\bar{q}$, in the apparent fractal regime ($\bar{q}_{gf} < \bar{q} < 1$), the intensity and structure factor decrease rapidly. Although both scattering functions in this region appear to scale as a power law, the scaling law exponent is not the mass-scaling exponent – $d_f = -2.4$, but is -2.0 ± 0.1. In fact, extracting a well-defined scaling exponent from the intermediate scale scattering regime is fraught with difficulty. It has been suggested that, by attempted linear fit on the log–log data plot starting at higher wavenumbers, one obtains a slope consistent with $d_f = 1.8$ associated with diffusion-limited cluster aggregation.[36] Nevertheless, there is a continuous variation in log slope that can be understood in terms of a cross-over from finite-size effects at small q to local particle structure at high q.[36–39] The true scaling regime where the mass-scaling relation can be measured with precision lies with the range $\bar{q}_{gf} \ll \bar{q} < 0.1$, which can be accessed only when the cluster size is extremely large. Our clusters of 50 000 are insufficiently large to unambiguously detect this regime.

At the largest $\bar{q}$, studied we see particle-scale nearest-neighbor correlations as bumps in the structure factor. These are particularly apparent for $\alpha = 1$, but less pronounced for long rods or thin disks. Particle shape plays an essential role in determining the nearest-neighbor distances between particle centers of mass, d_c, which must satisfy $1 \leq d_c/2a \leq \sqrt{1+\alpha^2}$ for $\alpha \geq 1$ and $\alpha \leq d_c/2a \leq \sqrt{1+\alpha^2}$ for $\alpha \leq 1$. For $\alpha = 1$, the relatively narrow distribution ($1 \leq d_c/2a \leq \sqrt{2}$) of d_c leads to the oscillatory behavior of $\bar{S}(\bar{q})$ at $\bar{q} > 1$, reminiscent of a liquid structure factor. The relative positions of the knee, when considered in combination with particle-scale features at higher- $\bar{q}$, can potentially be used to differentiate the aspect ratio of the constituent cylinders. Because at small r, the mass-scaling $V_T \sim r$ and $V_T \sim r^2$ for rod-like and disk-like cylinders, respectively (Fig. 3), the slope of $\bar{I}(\bar{q})$ for $\bar{q} > 1$ should approach -1 and -2 for $\alpha \gg 1$ and $\alpha \ll 1$, respectively (Fig. 6). To observe this, one must perform scattering measurements up to q that is large enough to probe the effective dimensionality of individual cylinders.

4 Discussion

Using anisotropic random-walker simulations, we have explored the effect of particle shape, as parameterized by the aspect ratio of right-circular cylinders, on the structure of clusters formed through DLA. We find that all such DLA clusters show the known mass scaling for DLA of spherical particles. However, given the same particle volume, clusters formed by DLA of long rods and thin disks are generically less dense than clusters formed by DLA of more compact particles, such as stubby cylinders. This is apparent both from the computed structure factor of the clusters and from their basic mass scaling.

While the fundamental self-affine scaling of the clusters obeys the expected power-law behavior at length scales that are much larger than the constituent particle size, the local structure of the clusters depends in detail on the aspect ratio of the cylinders. We find that the relative frequency of end–end bonds to body–body ones departs significantly from what would be naively expected based on the assumption that particles are equally likely to form bonds on all parts of their surfaces. We attribute this to the ability of the ends of cylinders, especially rods, to explore significantly more space than the area associated with the end-caps as the cylinders undergo anisotropic diffusion. Moreover, we find that particle shape controls the distribution of the number of interparticle contacts per particle in the cluster. The maximum of the nearest-neighbor distribution for long thin rods trends towards $z = 1$ in the limit of very high aspect ratios, and the cluster contains a dominant population of singly connected 'hair' in the periphery of the cluster. In addition, long rods offer

a greater opportunity for having larger coordination numbers than spheres or stubby cylinders simply because a long rod offers a target region that provides more accessible space for collisions with other rods.

A better understanding of the relationship between local particle connectivity and quasi-dimensionality may allow for the eventual control of DLA mesostructures composed of colloids having complex shapes. Such control could permit the optimization of their elastic, rheological, and electronic transport properties for specific applications. The present study about how the basic shape of the constituent colloids can influence larger assembled structures formed by non-equilibrium DLA provides insight into this general area.

The differences in local structures within the clusters as a function of α have implications for transport properties in materials containing diffusion-driven aggregates of cylinders. In particular, transport properties of DLA clusters made up of cylinders may be significantly different than those for DLA clusters of compact objects, such as spheres. For instance, electronic tunneling between nanotubes is strongly orientation dependent so that transport through clusters having many end–end contacts should be facilitated over transport through clusters having fewer such contacts. Since some nanotubes do not have solid end-caps, an interesting extension of this work would be to see if there are significant differences between clusters arising from DLA of solid cylinders, as compared to cylindrical tubes that have no end-caps. Examining the micromechanical properties of the clusters as a function of cylinder aspect ratio would be interesting, and altering the rigidity and type of bonding between cylinders could also lead to more compact structures having greater internal connectivity. Although the structure of a cylinder still retains a significant degree of symmetry, we have found a rich behavior in how the aspect ratio of the building blocks can influence structures formed through a classic DLA process. Anisotropic diffusion and increasing accessibility of multiple contact points both play a significant role, especially in determining the local nearest-neighbor structure. Exploring the diffusion-limited aggregation of more complex shapes than cylinders could provide additional insight into the role of particle shape in altering the cluster's structure.

Acknowledgements

The authors thank Frank Scheffold for enjoyable and helpful discussions regarding the work. AJL acknowledges the support of NSF (CMMI-0800533), and TGM acknowledges NSF (CHE-0450022).

References

1 T. A. Witten and L. M. Sander, *Phys. Rev. B: Condens. Matter Mater. Phys.*, 1983, **27**, 5686–5697.
2 B. M. Smirnov, *Phys. Rep.*, 1990, **188**, 1–78.
3 L. M. Sander, *Nature*, 1986, **322**, 789–793.
4 D. Risovic and M. Martinis, *J. Colloid Interface Sci.*, 1996, **182**, 199–203.
5 J. Blum, *Adv. Phys.*, 2006, **55**, 881–974.
6 P. Meakin and T. Vicsek, *Phys. Rev. A: At., Mol., Opt. Phys.*, 1985, **32**, 685–688.
7 B. B. Mandelbrot, A. Vespignani and H. Kaufman, *Europhys. Lett.*, 1995, **32**, 199–204.
8 C. R. Seager and T. G. Mason, *Phys. Rev. E: Stat., Nonlinear, Soft Matter Phys.*, 2007, **75**, 011406.
9 J. N. Wilking, S. M. Graves, C. B. Chang, K. Meleson, M. Y. Lin and T. G. Mason, *Phys. Rev. Lett.*, 2006, **96**, 015501.
10 S. Babu, J. C. Gimel and T. Nicolai, *Eur. Phys. J. E*, 2008, **27**, 297–308.
11 P. Meakin, *Phys. Rev. A: At., Mol., Opt. Phys.*, 1986, **33**, 3371–3382.
12 P. Meakin, Z.-Y. Chen and P. Evesque, *J. Chem. Phys.*, 1987, **87**, 630–635.
13 Y. Han and et al., *Science*, 2006, **314**, 626–630.
14 R. C. Ball, R. C. Brady, G. Rossi and B. R. Thompson, *Phys. Rev. Lett.*, 1985, **55**, 1406–1409.
15 H. J. Fan, P. Werner and M. Zacharias, *Small*, 2006, **2**, 700–717.
16 B. M. I. van der Zande, M. R. Böhmer, L. G. J. Fokkink and C. Schönenberger, *Langmuir*, 2000, **16**, 451–458.
17 N. B. Saleh, L. D. Pfefferle and M. Elimelech, *Environ. Sci. Technol.*, 2008, **42**, 7963–7969.
18 F. O. Morin, F. Rose, P. Martin, M. C. Tarhan, H. Kawakatsu and H. Fujita, *Nanoscale Res. Lett.*, 2007, **2**, 135–143.
19 Q. Wen and J. X. Tang, *Phys. Rev. Lett.*, 2006, **97**, 048101.
20 R. Bandyopadhyay and et al., *Phys. Rev. Lett.*, 2004, **93**, 228302.
21 T. G. Mason, *Phys. Rev. E: Stat., Nonlinear, Soft Matter Phys.*, 2002, **66**, 060402.
22 B. A. DiDonna and D. C. Morse, 2007, arXiv:cond-mat/0703418v1.
23 P. Meakin, *Phys. Rev. Lett.*, 1983, **51**, 1119–1122.
24 M. Kolb, R. Botet and R. Jullien, *Phys. Rev. Lett.*, 1983, **51**, 1123–1126.
25 J. C. Gimel, D. Durand and T. Nicolai, *Phys. Rev. B: Condens. Matter Mater. Phys.*, 1995, **51**, 11348–11357.
26 M. Doi and S. F. Edwards, *The Theory of polymer dynamics*, Oxford Press, Oxford, 1986.
27 J. G. Kirkwood and P. L. Auer, *J. Chem. Phys.*, 1951, **19**, 281–283.
28 W. Zhang and H. A. Stone, *J. Fluid Mech.*, 1998, **367**, 329–358.
29 P. Meakin, *Phys. Rev. A: At., Mol., Opt. Phys.*, 1983, **27**, 1495–1507; T. C. Halsey, *Phys. Rev. A: At., Mol., Opt. Phys.*, 1988, **38**, 4789–4793.
30 P. M. Chaikin and T. C. Lubensky, *Principles of condensed matter physics*, Academic Press, New York, 1995.
31 A. Pearson and R. W. Anderson, *Phys. Rev. B: Condens. Matter Mater. Phys.*, 1993, **48**, 5865–5885.
32 J. Kjems and T. Freltoft, in *Advances in Solid State Physics*, Springer, Berlin, 2007.
33 C. Allain and M. Cloitre, *Phys. Rev. B: Condens. Matter Mater. Phys.*, 1986, **33**, 3566–3569.
34 C. F. Bohren and D. R. Huffman, *Absorption and Scattering of Light by Small Particles*, Wiley-Interscience, New York, 1998.
35 R. F. Saraf, *Macromolecules*, 1989, **22**, 675–681.
36 C. Oh and C. M. Sorensen, *Phys. Rev. E: Stat., Nonlinear, Soft Matter Phys.*, 1998, **57**, 784–790.
37 W. G. Hanan and D. M. Heffernan, *Phys. Rev. E: Stat., Nonlinear, Soft Matter Phys.*, 2008, **77**, 011405.
38 M. Lattuada, H. Wu, A. Hasmy and M. Morbidelli, *Langmuir*, 2003, **19**, 6312–6316; M. Lattuada, H. Wu and M. Morbidelli, *Langmuir*, 2004, **20**, 4355–4362.
39 D. W. Schaefer, J. E. Martin, P. Wiltzius and D. S. Cannell, *Phys. Rev. Lett.*, 1984, **52**, 2371–2374.